Khan et al. *Boundary Value Problems* (2019) 2019:107
https://doi.org/10.1186/s13661-019-1221-1

Boundary Value Problems
a SpringerOpen Journal

REVIEW
Open Access

Parametric investigation of the Nernst–Planck model and Maxwell's equations for a viscous fluid between squeezing plates

Muhammad Sohail Khan[1*], Rehan Ali Shah[1], Amjad Ali[1] and Aamir Khan[1]

*Correspondence:
ph.sohail@uetpeshawar.edu.pk
[1]Department of Basic Sciences and Islamiat, University of Engineering and Technology Peshawar, Peshawar, Pakistan

Abstract

The Poisson–Boltzmann equation is derived from the assumption of thermodynamic equilibrium where the ionic distribution is not affected by fluid flow. Although this is a reasonable assumption for steady electroosmotic flow through straight micro-channels, there are some important cases where convective transport of ions has nontrivial effects. In these cases, it is necessary to adopt the Nernst–Planck equation instead of the Poisson–Boltzmann equation to model the internal electric field. The modeled system of equations is transformed by similarity transformation to derive the equations of flow field, electric potential, electrokinetic force, entropy generation, and energy equation. The Parametric Continuation Method (PCM) is used to solve the system of ordinary differential equations. It is concluded that decrease in the mass diffusion decreases the anion distribution from lower to upper plate. The Batchelor number decreases the strength of magnetic field. Entropy generation and the Bejan number are maximum near the two plates because of the maximum disorderness due to plate movements and have minimum value in the fluid's center. Also the Eckert number increases viscous heating, which causes the entropy production in the vicinity of the two plates to increase.

Keywords: Electric potential; Lorentz force; Entropy generation; Bejan number; Squeezing flow; Parametric continuation method

1 Introduction

In the analysis of electroosmotic flows, the internal electric potential is usually modeled by the Poisson–Boltzmann equation. The Poisson–Boltzmann equation is derived from the assumption of thermodynamic equilibrium where the ionic distribution is not affected by fluid flow. Although this is a reasonable assumption for steady electroosmotic flows through straight micro-channels, there are some important cases where convective transport of ions has nontrivial effects. In these cases, it is necessary to adopt the Nernst–Planck equation instead of the Poisson–Boltzmann equation to model the internal electric field. Hu [1] studied the steady electro-kinetic flow in squeezing channels in a T-shaped configuration. The nonlinear Poisson–Boltzmann equation for variable electro-kinetic radius and surface potential was numerically obtained. It was found that fluid flow can be controlled by applying a potential at each reservoir connected to the end of a channel. The inter-facial electro-kinetic effects on fluid flow through a micro-channel between parallel plates was studied by Mala [2]. Experiments were conducted to investigate the effects of electric double layer on flow characteristics with different potassium chloride concentrations in water and with different plate materials. The fluid flow through a micro-channel was also studied by Arulanumdum [3] through numerical methods. This investigation was bounded to the micro-channel flow in the fully developed region. The entry region effects were neglected and the charge density was assumed to be in the Boltzmann equilibrium distribution. Yang [4] investigated the entry flow effect induced by an applied electrical potential through micro-channel between parallel plates. The Nernst–Planck equation governing the ionic concentration distribution was numerically solved using a finite difference method.

Ferrohydrodynamics (FHD) deals with the mechanics of fluid motions influenced by strong forces of magnetic polarization. Magnetic fluids have several applications of heat transfer through ferrofluids. One such phenomenon is liquid-cooled speakers which involves small bulk quantities of the ferrofluid to conduct heat away from the speaker coils [1]. This innovation increases the amplifying power of the coil, and hence it leads to the loudspeaker producing high-fidelity sound. Another use of magnetic fluids is to bring the drugs to a targeted site in a human body, a magnetic field can pilot the path of a drop of ferrofluid in the human body [2]. Mutua [5] studied Stokes problem of a convective flow past a vertical infinite plate in a rotating system in the presence of variable magnetic field. They concluded that some or all of the parameters affect the fluid velocity and temperature. Consequently, their effect alters the rate of heat transfer and skin friction along the axes. Increase in magnetic parameter M and the Eckert number leads to an increase in the velocity profiles for both free convection cooling and heating at the plate. Seth [3] studied MHD flow and heat transfer along a porous flat plate with mass transfer and found that the fluid velocity component increased with an increasing value of time and Hall parameter, but decreased owing to an increasing value of transpiration parameter and magnetic field parameter. Victor [4] studied unsteady MHD free convection couette flow between two vertical permeable plates in the presence of thermal radiation using Galerkin's finite element method. It was found that the radiation parameter and the Prandtl number have a greater effect on the temperature than on the velocity. On the other hand, the magnetic parameter and the Grashof number have no effect on the fluid temperature. Gunakala [6] investigated unsteady MHD couette flow between two infinite parallel porous plates in an inclined magnetic field with heat transfer. The lower plate was considered to be porous and stationary. He found out that an increase in the magnetic number led to a decrease in the velocity of the fluid. Similarly the effect of magnetic field and heat transfer have also been studied in detail by [7–17].

The existing information on the topic witnesses that the electric potential and magnetic field dependent entropy generation of a viscous fluid between squeezing plates has never been reported and is the very first study in the literature. In the following sections, the problem is formulated, analyzed, and discussed through graphs and tables.

2 Formulation of the problem

Consider the axisymmetric and fully developed pressure driven flow of an incompressible elecroviscous fluid between the gap of the squeezing plates as shown in Fig. 1. The parallel plates are separated by a distance $a(t) = l\sqrt{1-\beta t}$, where l is the representative length

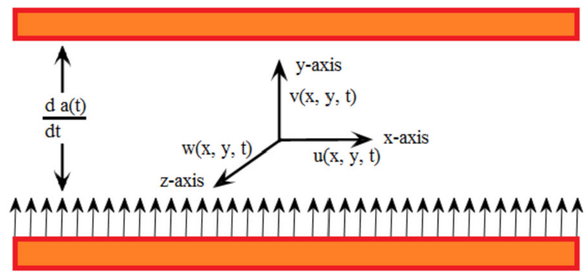

Figure 1 Geometry of the problem

equivalent to the plates separation at $t = 0$. Furthermore, we assume that fluid contains symmetric anions (+) and cations (−) with valencies $z_+ = -z_- = z = 1$, equal diffusivities $D_+ = D_- = D$ and that the bulk ion concentration of each ionic species is n_o. Electro-kinetic flows of fluid containing ionic species are described by the equation of continuity and the Navier–Stokes equations with an electrical body force term. These flow field equations are coupled with the Poisson equation relating the electrical potential to the charge distribution, and Nernst–Planck equations for conservation of each ion species. The induced magnetic field $(B_x, B_y, 0)$ in the fluid is generated by the applied magnetic field defined as

$$H_x = \frac{\beta r M_o}{\mu_2(1-\beta t)}, \qquad H_y = \frac{r N_o}{\mu_2(1-\beta t)},$$

where M_o and N_o are used to dimensionless H_x, H_y and μ_1, μ_2 are the magnetic permeabilities of outside and inside media between the two plates respectively. Following experimental study, the above parameters of magnetic field are zero on the lower plate [18].

The electro-kinematic flow equations have been nondimensionalized by introducing d, $\overline{\vartheta}$, $\frac{d}{\overline{\vartheta}}$, n_o, and $\frac{k_b T}{ze}$ as scaling variables for length, velocity, time, ion number density, and electrical potential, respectively, so the governing equations become as follows.

Continuity equation [7]:

$$\vec{\nabla}.\vec{u} = 0; \tag{1}$$

Momentum equation with electro-kinetic effect [7–11]:

$$\frac{\partial \vec{u}}{\partial t} + (\vec{u}.\vec{\nabla})\vec{u} = -\frac{1}{\rho}\vec{\nabla}\vec{p} + \nu\vec{\nabla}^2\vec{u} - \delta\left(n^+ - n^-\right)\vec{\nabla}\vec{U} + \vec{C}; \tag{2}$$

Magnetic induction equation [16, 17]

$$\frac{\partial \vec{C}}{\partial t} = \vec{\nabla} \times (\vec{u} \times \check{C}) + \frac{1}{\sigma \mu_e}\vec{\nabla}^2\vec{C}; \tag{3}$$

Poisson equation:

$$\vec{\nabla}^2\vec{U} = \frac{-1}{2}K_1^2\left(n^+ - n^-\right); \tag{4}$$

The Nernst–Plank equations [3–6, 18–26]:

$$\frac{\partial n^+}{\partial t} + \vec{\nabla}.(\vec{u}n^+) = \frac{\nu}{S_c}\big(\vec{\nabla}^2 n^+ + \vec{\nabla}.(n^+\vec{\nabla}\vec{U})\big), \tag{5}$$

$$\frac{\partial n^-}{\partial t} + \vec{\nabla}.(\vec{u}n^-) = \frac{\nu}{S_c}\big(\vec{\nabla}^2 n^- + \vec{\nabla}.(n^-\nabla U)\big); \tag{6}$$

Equations of energy [12–17]:

$$\rho C_p\left(\frac{\partial \bar{T}}{\partial t} + \vec{u}.\vec{\nabla}T\right) = \kappa\vec{\nabla}^2\vec{T} + Trac(T.L), \tag{7}$$

where $\aleph_e$ is the Reynolds number, S_{ch} is the Schmidt number, D is ion diffusivity, z is valency, e is elementary charge, k_B is the Boltzmann constant, T is absolute temperature, U is local total electrical potential induced by ions, ϵ_o is the permittivity of vacuum, ϵ is a dielectric constant, d is the distance between disks, ς_o is the surface electric potential at a reference position, κ_d is an inverse Debye constant, B is fixed for a given fluid at a constant temperature, and n^+, n^- are the number per unit volume of anions and cations, respectively.

3 Boundary conditions

The boundary conditions are chosen as follows:

$$\begin{aligned}
&u = v = 0, \qquad U = 0, \qquad n^+ = c_1, \qquad n^- = 0,\\
&\quad \beta_0 = 0, \qquad b = 0, \qquad T = 0 \quad \text{at } y = 0,\\
&u = 0, \qquad v = -\frac{\beta l}{2\sqrt{1-\beta t}}, \qquad U = \frac{x}{l\sqrt{1-\beta t}}, \qquad n^+ = 0, \qquad n^- = \frac{n_0}{1-\beta t},\\
&\quad \beta_0 = \frac{\mu}{l\sqrt{1-\beta t}}, \qquad b = \frac{x\mu}{l^2(1-\beta t)}, \qquad T = T_h \quad \text{at } y = h(t),
\end{aligned} \tag{8}$$

where n_w is the outward unit vector normal to the disks surface, s_{cd} is the dimensionless surface charge density, and Ψ is the total electric potential.

The following similarity transformations [16, 17] are chosen for reducing the partial differential Eqs. (1)–(7) to a system of ordinary differential equations:

$$\begin{aligned}
&u = \frac{\beta x}{2(1-\beta t)}f'(\eta), \qquad v = -\frac{\beta l}{\sqrt{1-\beta t}}f(\eta), \qquad \beta_0 = \frac{\mu}{l\sqrt{1-\beta t}}M(\eta),\\
&b = \frac{x\mu}{l^2(1-\beta t)}N(\eta), \qquad n^+ = \frac{n_0}{1-\beta t}H(\eta),\\
&n^- = \frac{n_0}{1-\beta t}K(\eta), \qquad U = \frac{xP(\eta)}{l\sqrt{1-\beta t}}, \qquad T = T_h\theta(\eta), \quad \text{where } \eta = \frac{y}{l\sqrt{1-\delta t}}.
\end{aligned} \tag{9}$$

Equation (1) is identically satisfied and Eqs. (2)–(7) take the following form:

$$\begin{aligned}
f'''' = {}& S\big(2f'' + \eta f''' + f'f'' - ff'''\big)\\
&- BK_1^2\sqrt{\delta}\big[\alpha_2\big(P'H - P'K\big) + \alpha_1\big(P'H + PH' - P'K - PK'\big)\big]\\
&- 2M'f'' - Mf''' - f''N - 2f'N' - S^2Bt\big(Mf' + \eta M'f'\big) - BtS\big(ff'N + f'^2M\big)
\end{aligned}$$

$$- S^2Bt\big(2fN + \eta fN'\big) + BtS\big(ff''M + ff'M' + ff'N + f^2N'\big), \tag{10}$$

$$N'' = S^2Bt\big(2N + \eta N'\big) - BtS\big(Mf'' + f'M' + f'N + fN'\big), \tag{11}$$

$$M'' = S^2Bt\big(M + \eta M'\big) + BtS\big(fN + f'M\big), \tag{12}$$

$$P'' = -\frac{1}{2}K_2^2\sqrt{\delta}(H - K), \tag{13}$$

$$H'' = SS_c\big(2H + \eta H' - fH'\big) - \frac{1}{\sqrt{\delta}}\left[P'H' - \frac{1}{2}K_2^2\sqrt{\delta}\big(H^2 - KH\big)\right], \tag{14}$$

$$K'' = SS_c\big(2K + \eta K' - fK'\big) - \frac{1}{\sqrt{\delta}}\left[P'K' - \frac{1}{2}K_2^2\sqrt{\delta}\big(KH - K^2\big)\right], \tag{15}$$

$$\theta'' = PrS\big(\eta\theta' - f\theta'\big) + PrEc\big(4\delta f'^2 + f''^2\big), \tag{16}$$

and the boundary conditions are reduced to

$$\begin{aligned} &f(0) = 0, \quad f'(0) = 0, \quad P(0) = 0, \quad H(0) = c_1, \quad K(0) = 0, \\ &N(0) = 0, \quad M(0) = 0, \quad \theta(0) = 0 \\ &f(1) = 0.5, \quad f'(1) = 0, \quad P(1) = 1, \quad H(1) = 0, \quad K(1) = 1, \\ &N(1) = 1, \quad M(1) = 1, \quad \theta(1) = 1, \end{aligned} \tag{17}$$

where $S = \frac{\beta l^2}{2\nu}$ is the squeeze number, $Sc = \frac{\mu}{\rho D}$ is the Schmidt number, $Bt = \sigma\mu_0\nu$ is the Batchelor number, $P_r = \frac{\mu C_p}{\kappa}$ is the Prandtl number, $Ec = \frac{1}{C_p T_h}[\frac{\beta x}{2(1-\beta t)}]^2$ is the Eckert number, $\delta = \frac{l^2(1-\beta t)}{x^2}$, $B = \frac{\rho k^2 T^2 \varepsilon_0 \varepsilon}{2z^2e^2\mu^2}$, $K_1^2 = \frac{2z^2e^2n_0}{\varepsilon_0\varepsilon k_b T}$, $K_2^2 = \frac{2z^2e^2l^2n_0}{\varepsilon_0\varepsilon k_b T}$, $\alpha_1 = \frac{2un_0}{\beta\rho}$, $\alpha_1 = \frac{2xun_0}{\beta\rho}$, and $\lambda = \frac{l^2}{\mu\mu_0}$.

4 Entropy generation

The volumetric rate of local entropy generation, in the case of the existence of a magnetic field, can be expressed in the following form [27]:

$$N_s = \frac{\kappa}{T_\infty^2}(\nabla T)^2 + \frac{T : \nabla V}{T_\infty} + \frac{1}{T_\infty}\big[(J - QC)(E + V \times C)\big], \tag{18}$$

which can be expressed in its dimensionless form by the following expression:

$$\begin{aligned} N_g = {}& \frac{\kappa}{T_\infty^2 l^2}\left[\left(\frac{\partial T}{\partial x}\right)^2 + \left(\frac{\partial T}{\partial y}\right)^2\right] + \frac{\mu}{T_\infty}\left[4\left(\frac{\partial \vec{u}}{\partial x}\right)^2 + \left(\frac{\partial \vec{u}}{\partial y} + \frac{\partial \vec{v}}{\partial x}\right)^2\right] \\ & + \frac{1}{T_\infty}\sigma\big[u^2B_0^2 - 2uvbB_0 + v^2b^2\big]. \end{aligned} \tag{19}$$

After transformation it can be written as

$$Ns = \theta'^2 + \Omega PrEc\big(4\delta f'^2 + f''^2\big) + \frac{\Omega PrEcBt\lambda}{S}\big(f'^2M^2 + f^2N^2 + 2ff'MN\big), \tag{20}$$

where T_∞ is a reference temperature, κ is the thermal conductivity, Q is the electric charge density, J is the electric current, E is the electric field, V is the velocity vector, the entropy generation rate is $Ns = \frac{N_g}{N_{g0}}$, the characteristic entropy generation rate is $N_{g0} = \frac{k_{nf}T_H}{T_\infty^2 a^2}$, the dimensionless temperature difference is $\Omega = \frac{T_\infty}{T_H}$, respectively. Therefore the local entropy generation in a dimensionless form can be written as

$$Ns = N_H + N_f + N_{mf}, \tag{21}$$

where the local entropy generation due to heat transfer is N_H, the local entropy generation due to fluid friction is N_f, and the local entropy generation due to magnetic field is N_{mf}. In order to get the idea of relative importance of heat transfer effects and viscous effects, the Bejan number is defined:

$$Be = \frac{N_H}{Ns} = \frac{\theta'^2}{\theta'^2 + \Omega PrEc(4\delta f'^2 + f''^2) + \frac{\Omega PrEcBt\lambda}{S}(f'^2M^2 + f^2N^2 + 2ff'MN)}. \tag{22}$$

In the absence of magnetic field ($G = H = 0$), Eqs. (14)–(16) were solved.

Physical quantities of interest are the skin friction coefficient and the Nusselt number which are defined as follows:

$$C_f = \frac{\mu(\frac{\partial u}{\partial y})_{y=h(t)}}{\rho \upsilon^2}, \qquad N_u = \frac{-lk(\frac{\partial T}{\partial y})_{y=h(t)}}{kT_h}. \tag{23}$$

It terms of Eq. (13), we obtain

$$\frac{2\nu(1-\beta t)^{\frac{3}{2}}}{\beta x} C_f = f''(1), \qquad (1-\beta t)^{\frac{1}{2}} N_u = -\theta'(1). \tag{24}$$

5 Analytic solution by parametric continuation method

Application of the parametric continuation method to nonlinear equations (10)–(16) with boundary conditions in Eq. (17) and optimal choice of continuation parameter is applied in this section. The following algorithm is presented as a sequence of steps to be followed for the application of this method.

- *Canonical form of BVP as a first order ODE.* To convert Eqs. (10)–(16) into a first order ODE, suppose the following:

$$\begin{aligned} &f = h_1, \quad f' = h_2, \quad f'' = h_3, \quad f''' = h_4, \\ &N = h_5, \quad N' = h_6, \quad M = h_7, \quad M' = h_8, \\ &P = h_9, \quad P' = h_{10}, \quad H = h_{11}, \quad H' = h_{12}, \\ &K = h_{13}, \quad K' = h_{14}, \quad \theta = h_{15}, \quad \theta' = h_{16}. \end{aligned} \tag{25}$$

By putting these transformations in Eqs. (10)–(16), they become

$$\begin{aligned} h_4' = {} & S(2h_3 + \eta h_4 + h_2h_3 - h_1h_4) \\ & - BK_1^2\sqrt{\delta}\big[\alpha_2(h_{10}h_{11} - h_{10}h_{13}) + \alpha_1(h_{10}h_{11} + h_9h_{12} - h_{10}h_{13} - h_9h_{14})\big] \\ & - 2h_8h_3 - h_7h_4 - h_3h_5 + 2h_2h_6 \\ & + S^2Bt(h_2h_7 + \eta h_2h_8) + BtS\big(h_1h_2h_5 + h_2^2h_7\big) + S^2Bt(2h_1h_5 + \eta h_1h_6) \\ & - BtS\big(h_1h_3h_7 + h_1h_2h_8 + h_1h_2h_5 + h_1^2h_6\big), \end{aligned} \tag{26}$$

$$h_6' = S^2Bt(\eta h_6 + 2h_5) - BtS(h_3h_7 + h_2h_8 + h_2h_5 + h_1h_6), \tag{27}$$

$$h_8' = S^2Bt(\eta h_8 + h_7) + BtS(h_1h_5 + h_2h_7), \tag{28}$$

$$h_{10}' = -\frac{1}{2}BK_2^2\sqrt{\delta}(h_{11} - h_{13}), \tag{29}$$

$$h_{12}' = ScS(2h_{11} - \eta h_{12} - h_1h_{12}) - \frac{1}{\sqrt{\delta}}\left[h_{10}h_{12} - \frac{1}{2}BK_2^2\sqrt{\delta}\left(h_{11}^2 - h_{11}h_{13}\right)\right], \tag{30}$$

$$h_{14}' = ScS(2h_{13} - \eta h_{14} - h_1h_{14}) - \frac{1}{\sqrt{\delta}}\left[h_{10}h_{14} - \frac{1}{2}BK_2^2\sqrt{\delta}\left(h_{13}^2 - h_{11}h_{13}\right)\right], \tag{31}$$

$$h_{16}' = PrS(\eta h_{16} - h_1h_{16}) + PrEc\left(4\delta h_2^2 + h_3^2\right) \tag{32}$$

and the boundary conditions become

$$\begin{aligned} &h_2(0) = 0, \quad h_1(0) = 0, \quad h_2(1) = 0, \quad h_1(1) = 1, \quad h_5(0) = 0, \\ &h_5(1) = 1, \quad h_7(0) = 0, \quad h_7(1) = 1, \quad h_9(0) = 0, \quad h_9(1) = 1, \\ &h_{11}(0) = c1, \quad h_{11}(1) = 0, \quad h_{13}(0) = 0, \quad h_{13}(1) = 1, \\ &h_{15}(0) = 0, \quad h_{15}(1) = 1. \end{aligned} \tag{33}$$

- *Introduction of a parameter p and imbedding of the obtained ODE in a p-parameter family.* To obtain ODE in a p-parameter family, let us introduce the p-parameter in Eqs. (18)–(24), and so

$$\begin{aligned} h_4' = {} & S\left[2h_3 + \eta h_4 + h_2h_3 - h_1(h_4 - 1)p\right] \\ & - BK_1^2\sqrt{\delta}\left[\alpha_2(h_{10}h_{11} - h_{10}h_{13}) + \alpha_1(h_{10}h_{11} + h_9h_{12} - h_{10}h_{13} - h_9h_{14})\right] \\ & - 2h_8h_3 - h_7h_4 - h_3h_5 + 2h_2h_6 \\ & + S^2Bt(h_2h_7 + \eta h_2h_8) + BtS\left(h_1h_2h_5 + h_2^2h_7\right) + S^2Bt(2h_1h_5 + \eta h_1h_6) \\ & - BtS\left(h_1h_3h_7 + h_1h_2h_8 + h_1h_2h_5 + h_1^2h_6\right), \end{aligned} \tag{34}$$

$$h_6' = S^2Bt(\eta h_6 + 2h_5) - BtS\left[h_3h_7 + h_2h_8 + h_2h_5 + h_1(h_6 - 1)p\right], \tag{35}$$

$$h_8' = S^2Bt\left[\eta(h_8 - 1)p + h_7\right] + BtS(h_1h_5 + h_2h_7), \tag{36}$$

$$h_{10}' = -\frac{1}{2}BK_2^2\sqrt{\delta}\left[h_{11} - h_{13} + h_{10} - (h_{10} - 1)p\right], \tag{37}$$

$$\begin{aligned} h_{12}' = {} & ScS\left[2h_{11} - \eta h_{12} - h_1(h_{12} - 1)p\right] \\ & - \frac{1}{\sqrt{\delta}}\left[h_{10}h_{12} - \frac{1}{2}BK_2^2\sqrt{\delta}\left(h_{11}^2 - h_{11}h_{13}\right)\right], \end{aligned} \tag{38}$$

$$\begin{aligned} h_{14}' = {} & ScS\left[2h_{13} - \eta h_{14} - h_1(h_{14} - 1)p\right] \\ & - \frac{1}{\sqrt{\delta}}\left[h_{10}h_{14} - \frac{1}{2}BK_2^2\sqrt{\delta}\left(h_{13}^2 - h_{11}h_{13}\right)\right], \end{aligned} \tag{39}$$

$$h_{16}' = PrS\left[\eta h_{16} - h_1(h_{16} - 1)p\right] + PrEc\left(4\delta h_2^2 + h_3^2\right). \tag{40}$$

- *Differentiation by p leads to the following system with respect to sensitivities to the parametric p.* Differentiate Eqs. (26)–(32) with respect to p

$$V_1' = A_1 V_1 + R_1, \tag{41}$$

where A_1 is a coefficient matrix, R_1 is a remainder, and $V_1 = \frac{dh_i}{d\tau}$, $1 \leq i \leq 16$.
- *Application of the supposition principle and specifying the Cauchy problem for each component*

$$V_1 = aU + W_1. \tag{42}$$

Here U, W_1 are unknown vector functions. Solving the following two Cauchy problems for each component, we satisfy then automatically the original ODE

$$(aU + W_1)' = A_1(aU + W_1) + R_1 \tag{43}$$

and left boundary conditions.
- *Numerical solution of Cauchy problem.* An implicit scheme is used for the solution of this problem as follows:

$$\frac{U^{i+1} - U^i}{\triangle\eta} = A_1 U^{i+1}, \tag{44}$$

$$\frac{W^{i+1} - W^i}{\triangle\eta} = A_1 W^{i+1} + R_1. \tag{45}$$

- *Selection of corresponding blend coefficient.* Since given boundary conditions are applied only for h_i, where $1 \leq i \leq 16$, when solving ODE for sensitivities, we need to apply $V_2 = 0$, which in a matrix form looks as

$$J_1.V_1 = 0 \quad \text{or} \quad J_1.(aU + W_1) = 0, \tag{46}$$

where $a = \frac{-J_1.W_1}{J_1.U}$.

6 Results and discussions

The mathematical formulation for the constitutive expressions of unsteady Newtonian fluid is employed to model the flow between the rectangular space of squeezing plates in the form of Eqs. (10)–(16) subject to the boundary conditions given in Eq. (17). These equations are solved and compared for numerical investigations through PCM and BVP4*c*. Parametric analysis is carried out for the dimensionless involved physical parameters. The effects of these parameters are shown in the form of Tables 1–2 and Figs. 2–13. The squeeze Reynolds number S is the ratio between the normal velocity of the upper plate and kinematic viscosity of the fluid. It is important to note that small or big values of S mean slow or rapid vertical velocity of the upper plate toward the lower plate. Positive values of S also mean that the upper plate is moving away from the lower plate, or the increase in the distance between the plates where negative values of S mean that the upper plate is moving toward the lower plate, or decrease of distance between the plates.

Table 1 Comparison of the different values of $f''(\eta)$, $N'(\eta)$, $M'(\eta)$, $m'(\eta)$, $H'(\eta)$, $K'(\eta)$, and $\theta'(\eta)$ using the parametric continuation method approximation for the case $Sc = 1.5$, $\delta = 1.0$, $\alpha_1 = 1.2$, $\alpha_2 = 1.8$, $Bt = 0.3$, $B = 1.7$, $K_1 = 1.8$, $K_2 = 2.6$, $Pr = 0.6$, $Ec = 0.3$

S	$f''(1)$	$N'(1)$	$M'(1)$	$m'(1)$	$H'(1)$	$K'(1)$	$\theta'(1)$
0.2	–4.4659	1.0031	1.0378	1.8676	–0.5952	0.1377	2.2402
0.4	–4.5614	1.0295	1.0915	1.8390	–0.5413	0.3469	2.2451
0.6	–4.6585	1.0784	1.1611	1.8133	–0.4945	0.5409	2.2505
0.8	–4.7573	1.1494	1.2467	1.7900	–0.4536	0.7222	2.2564
1	–4.8580	1.2419	1.3487	1.7686	–0.4175	0.8926	2.2628

Table 2 Comparison of the different values of $f''(\eta)$, $N'(\eta)$, $M'(\eta)$, $m'(\eta)$, $H'(\eta)$, $K'(\eta)$, and $\theta'(\eta)$ using the parametric continuation method approximation for the case $Sc = 1.5$, $\delta = 1.0$, $\alpha_1 = 1.2$, $\alpha_2 = 1.8$, $Bt = 0.3$, $B = 1.7$, $K_1 = 1.8$, $K_2 = 2.6$, $Pr = 0.6$, $Ec = 0.3$, $\Omega = 1.2$, $\lambda = 0.3$

S	$Ns(1)$	$Be(1)$	Pr	$Ns(1)$	$Be(1)$	Ec	$Ns(1)$	$Be(1)$	Ω	$Ns(1)$	$Be(1)$
0.2	9.4238	0.5325	0.2	2.0260	0.6531	0.2	5.3760	0.6095	0.1	5.4411	0.9035
0.4	9.5832	0.5260	0.4	5.3812	0.6099	0.4	11.0860	0.6213	0.1	5.9659	0.8241
0.6	9.7846	0.5176	0.6	8.0652	0.6096	0.6	18.1219	0.6525	0.1	6.4908	0.7574
0.8	10.0041	0.5089	0.8	11.0781	0.6210	0.8	26.4837	0.6829	0.1	7.0156	0.7008
1	10.2372	0.5002	1	14.4195	0.6360	1	36.1715	0.7098	0.1	7.5404	0.6520

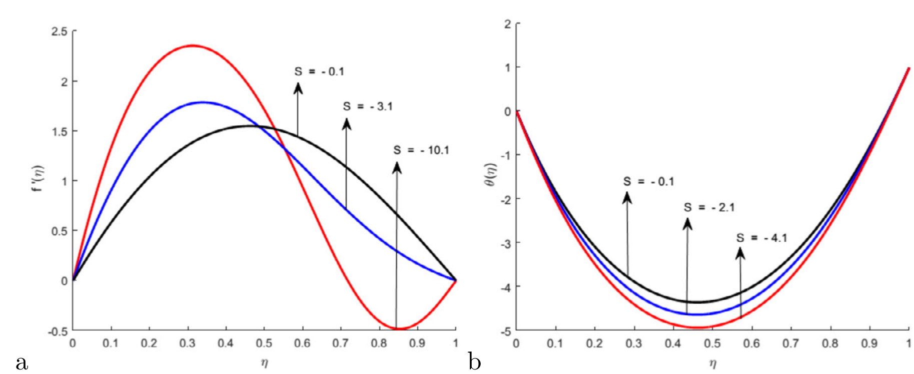

Figure 2 Profile of $f'(\eta)$ and $\theta(\eta)$ for different values of S and fixed values of $Sc = 1.5$, $\delta = 1.0$, $\alpha_1 = 1.2$, $\alpha_2 = 1.8$, $Bt = 0.3$, $B = 1.7$, $K_1 = 1.8$, $K_2 = 0.6$, $Pr = 1.6$, $Ec = 0.5$

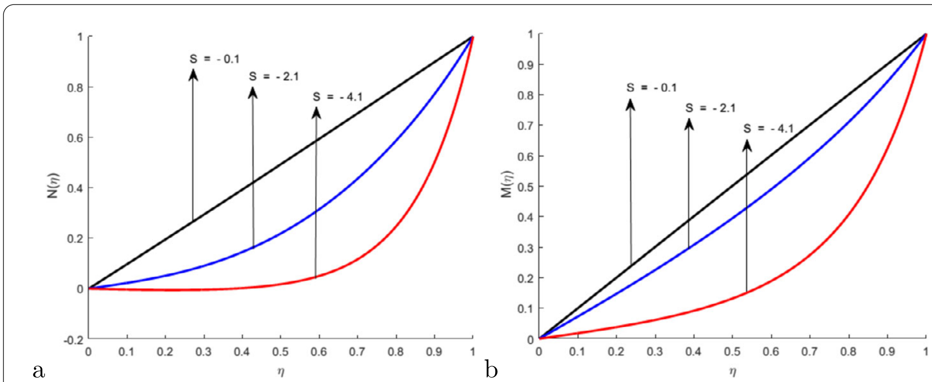

Figure 3 Profile of $N(\eta)$ and $M(\eta)$ for different values of S and fixed values of $Sc = 1.5$, $\delta = 2.0$, $\alpha_1 = 1.2$, $\alpha_2 = 0.4$, $Bt = 0.3$, $B = 1.7$, $K_1 = 1.8$, $K_2 = 2.6$, $Pr = 0.6$, $Ec = 3.5$

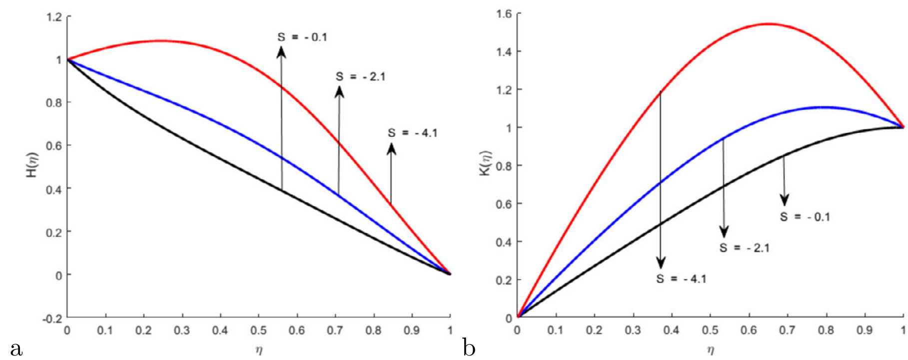

Figure 4 Profile of $H(\eta)$ and $K(\eta)$ for different values of S and fixed values of $Sc = 0.5$, $\delta = 2.0$, $\alpha_1 = 1.2$, $\alpha_2 = 0.4$, $Bt = 0.3$, $B = 1.7$, $K_1 = 1.8$, $K_2 = 2.6$, $Pr = 0.6$, $Ec = 3.5$

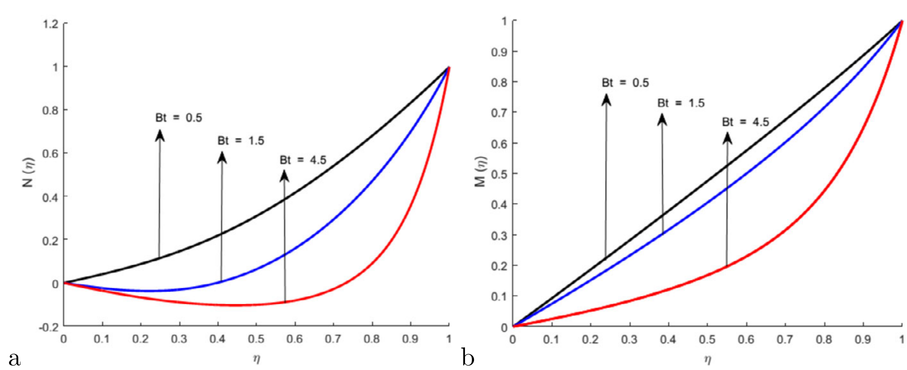

Figure 5 Profile of $N(\eta)$ and $M(\eta)$ for different values of B_t and fixed values of $Sc = 1.5$, $\delta = 4.0$, $\alpha_1 = 1.2$, $\alpha_2 = 1.8$, $B = 1.7$, $S = -1.1$, $K_1 = 1.8$, $K_2 = 2.6$, $Pr = 1.6$, $Ec = 0.5$

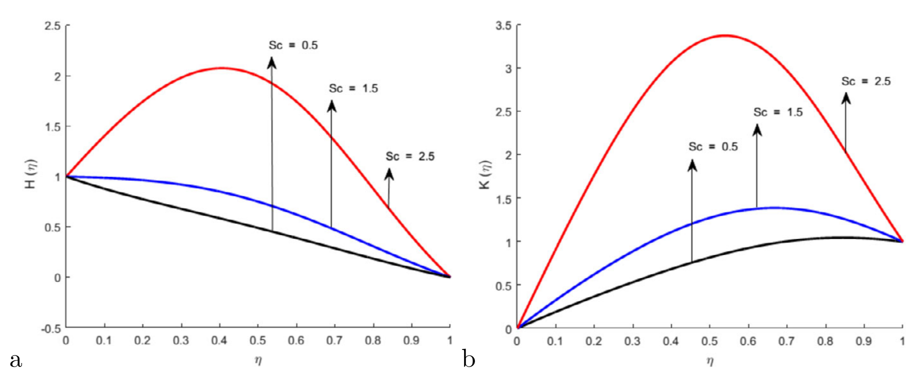

Figure 6 Profile of $H(\eta)$ and $K(\eta)$ for different values of S_c and fixed values of $Bt = 0.3$, $\delta = 4.0$, $\alpha_1 = 1.2$, $\alpha_2 = 1.8$, $B = 1.7$, $S = -1.1$, $K_1 = 1.8$, $K_2 = 2.6$, $Pr = 1.6$, $Ec = 0.5$

Figures 2 and 3 are made to depict the influence of squeeze Reynolds number S on the horizontal component of velocity field. It is clear from Fig. 2(a) that moving the upper plate toward the lower one pushes the fluid in horizontal direction. Increase in the normal velocity ($S = -0.1, -3.1, -10.1$) of the upper plate toward the lower plate is creating

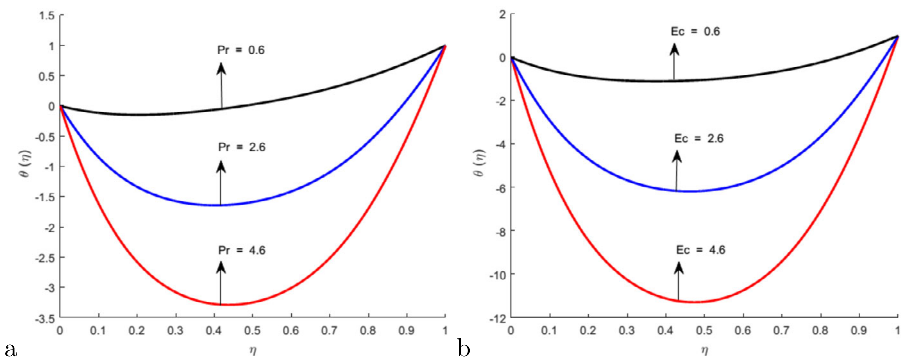

Figure 7 Profile of $\theta(\eta)$ for different values of P_r, E_c and fixed values of $Sc = 1.5$, $Bt = 0.3$, $\delta = 4.0$, $\alpha_1 = 1.2$, $\alpha_2 = 1.8$, $B = 1.7$, $S = -1.1$, $K_1 = 1.8$, $K_2 = 2.6$

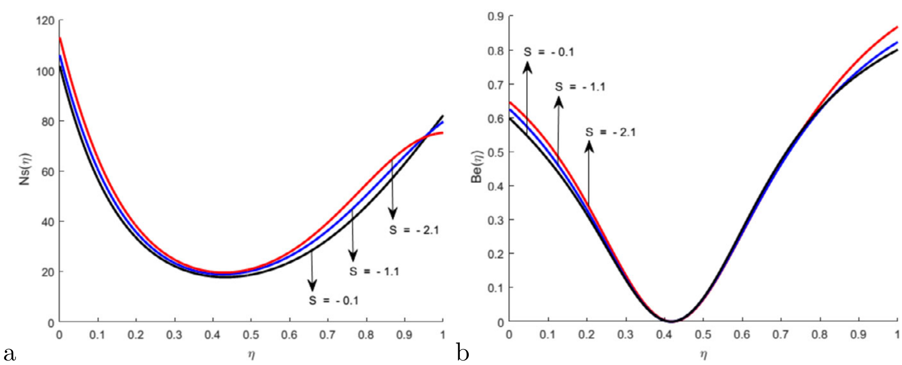

Figure 8 Profile of $N_s(\eta)$ and $B_e(\eta)$ for different values of S and fixed values of $Sc = 0.5$, $\delta = 2.0$, $\alpha_1 = 1.2$, $\alpha_2 = 0.4$, $Bt = 0.3$, $B = 1.7$, $K_1 = 1.8$, $K_2 = 2.6$, $Pr = 1.6$, $Ec = 0.5$, $\Omega = 1.2$, $\lambda = 0.3$

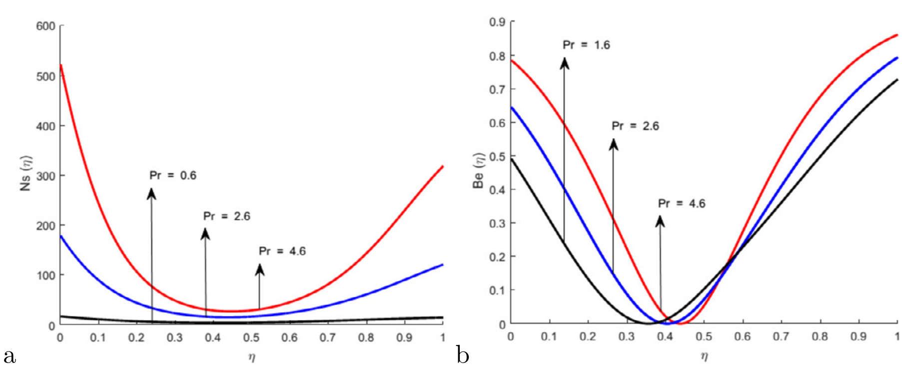

Figure 9 Profile of $N_s(\eta)$ and $B_e(\eta)$ for different values of P_r, E_c and fixed values of $Sc = 1.5$, $Bt = 0.3$, $\delta = 4.0$, $\alpha_1 = 1.2$, $\alpha_2 = 1.8$, $B = 1.7$, $S = -1.1$, $K_1 = 1.8$, $K_2 = 2.6$, $\Omega = 1.2$, $\lambda = 0.3$, $Ec = 0.5$

an opposing force to the vertical component, and so the fluid tends to move in horizontal direction. The effect of this normal velocity dominates the vertical velocity near the lower plate. However, as fluid crosses the central region, the vertical velocity overcomes the horizontal velocity and so $f'(\eta)$ starts decreasing. The effect of S is also investigated for temperature distribution as shown in Fig. 2(b). The temperature at upper plate at $\eta = 1$

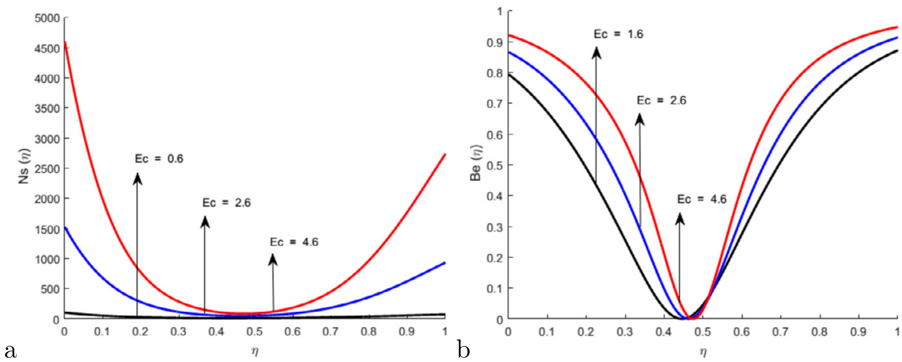

Figure 10 Profile of $N_s(\eta)$ and $B_e(\eta)$ for different values of E_c and fixed values of $Sc = 1.5$, $Bt = 0.3$, $\delta = 4.0$, $\alpha_1 = 1.2$, $\alpha_2 = 1.8$, $B = 1.7$, $S = -1.1$, $K_1 = 1.8$, $K_2 = 2.6$, $\Omega = 1.2$, $\lambda = 0.3$, $Pr = 1.6$

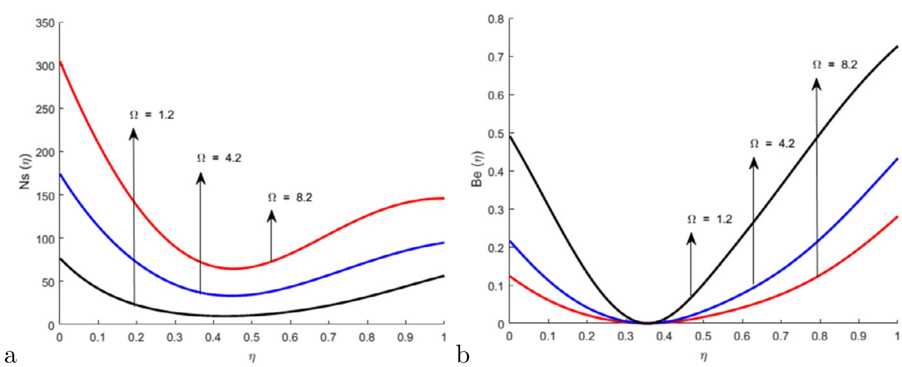

Figure 11 Profile of $N_s(\eta)$ and $B_e(\eta)$ for different values of Ω and fixed values of $Sc = 1.5$, $Bt = 0.3$, $\delta = 4.0$, $\alpha_1 = 1.2$, $\alpha_2 = 1.8$, $B = 1.7$, $S = -1.1$, $K_1 = 1.8$, $K_2 = 2.6$, $Ec = 0.5$, $\lambda = 0.3$, $Pr = 1.6$

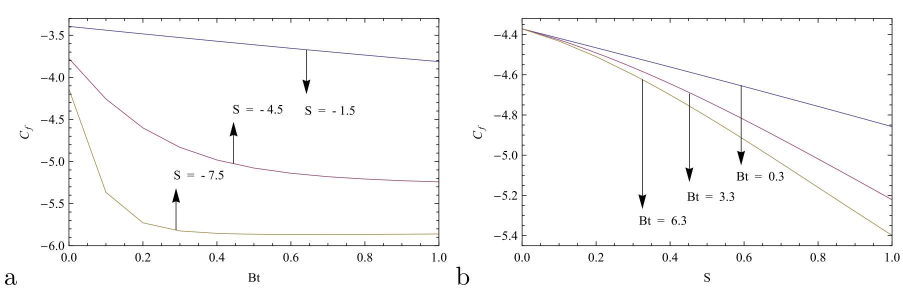

Figure 12 (**a**) The effect of skin friction for different values of S. (**b**) The effect of skin friction for different values of Bt. With fixed values are $Sc = 1.5$, $Bt = 0.3$, $\delta = 1.0$, $\alpha_1 = 1.2$, $\alpha_2 = 1.8$, $B = 1.7$, $S = -1.1$, $K_1 = 1.8$, $K_2 = 2.6$, $\Omega = 1.2$, $\lambda = 0.3$, $Ec = 0.3$, $Pr = 0.6$

is 1, and so by diffusion it is deceasing from layer to layer toward the lower plate. This decrease in temperature starts increasing after the central region due to decrease in fluid's kinetic viscosity.

The effect of S on magnetic field components $M(\eta)$ and $N(\eta)$ is shown in Fig. 3. An increase in the magnitude of squeeze Reynolds number S leads to decrease in kinetic viscosity of the fluid. This decrease in kinetic viscosity means an increase in the fluid's density,

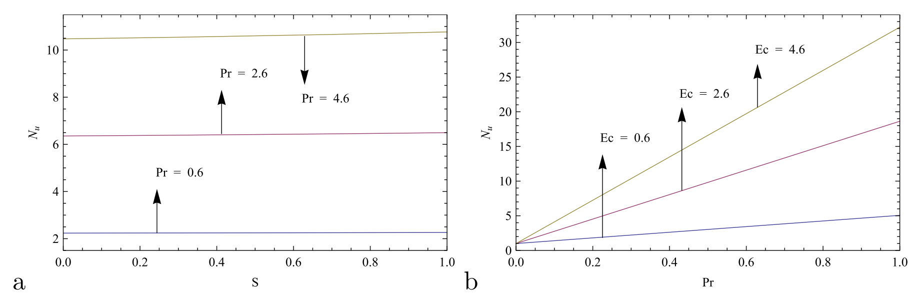

Figure 13 (**a**) The effect of Nusselt number for different values of *Pr*. (**b**) The effect of Nusselt number for different values of *Ec*. With fixed values are $Sc = 1.5$, $Bt = 0.3$, $\delta = 1.0$, $\alpha_1 = 1.2$, $\alpha_2 = 1.8$, $B = 1.7$, $S = -1.1$, $K_1 = 1.8$, $K_2 = 2.6$, $\Omega = 1.2$, $\lambda = 0.3$, $Ec = 0.3$, $Pr = 0.6$

which gives strength to the magnetic field from the lower to the upper plate as depicted in Fig. 3(*a*–*b*). Similarly this increase in density gives strength to the electric field because a strong magnetic field could be created due to strong electric field. Figure 4(*a*–*b*) clearly show that the cations distribution is getting stronger from the lower to the upper plate.

Figure 5 is made to investigate the effect of Batchelor number B_t on magnetic field components. The Batchelor number B_t for moderate values of the squeeze Reynolds number S is a measure of how easily the fluid slips from the magnetic field. When B_t is very large, a small current will create a large induced magnetic field. When B_t is very small, moderate-sized currents will only produce induced fields, which essentially have small perturbations on the applied field [28]. Clearly Fig. 5*a* shows that an increase in B_t decreases the horizontal component of magnetic field. This is due to the fact that magnetic field effect is weaker near the lower plate which is getting stronger as fluid moves toward the upper plate.

The effect of Schmidt number S_c on $H(\eta)$ and $K(\eta)$ is depicted in Fig. 6. The Schmidt number is the ratio of the momentum to the mass diffusivities. An increase in S_c means increase in momentum or decrease in the mass diffusion. It is noticed that decreasing the mass diffusion is decreasing the anion distribution from the lower to the upper plate. Also it can be seen that near the lower plate, the anion distribution increases with increase in the Schmidt number due to smaller mass diffusion with greater S_c. The influence of P_r and E_c on temperature distribution $\theta(\eta)$ is depicted in Fig. 7. The Prandtl number is the ratio of momentum and thermal diffusivities. It is noticed that increase in P_r causes decrease in temperature because of decrease in thermal diffusion. The temperature is increasing after the central region because of heat diffusion from the upper plate at $\eta = 1$. Similarly an increase in E_c means increase in the kinetic energy of fluid molecules which is maximum near the upper plate due to their motion.

Figures 8–12 are made to study the entropy generation and the Bejan number of squeezing flow for the effect of different involved parameters. The effect of squeezing parameter is depicted in Fig. 9. It is investigated that both entropy and Bejan number are maximum near the two plates because of the maximum disorderness due to plate movements and have minimum value in the center at $\eta = 0.5$. The effects of Prandtl number and Eckert number on $Ns(\eta)$ and $Be(\eta)$ are almost same and are shown in Figs. 9–10. An increase in the Prandtl number means an increase in the momentum diffusivity that reaches its maximum value near the two movable plates. The pace of this diffusion is in the descending order from one layer to the other, which clearly shows that the rate of the entropy generation and the Bejan number are maximum near the adjacent plate due to maximum disorderness of molecules and are minimum in the middle of the liquid domain. An increase in Ω increases the rate of the entropy generation due to the thermal propagation (due to the friction of liquid and plates) of the moving plates. This thermal diffusion is higher near the plates, and so the entropy generation rate decreases gradually from one layer to another, and thus constitutes the minimum in the center of the liquid domain as shown in Fig. 11. Results of physical interest for the skin friction and the Nusselt number for different values of S, B_t, P_r, and E_c are plotted in Figs. 12–13. Here it is shown that the skin friction decreases with an increase in S, while the heat transfer increases with an increase in S. The reason is that heat generation increases with increase in S due to collision of molecules. Also this phenomenon increases the fluid velocity due to which the skin friction decreases. No change is noticed for the Prandtl number on skin.

7 Concluding remarks

The mathematical formulation for the constitutive expressions of unsteady Newtonian fluid is employed to model the flow between the rectangular space of porous and squeezing plates in the form of Eqs. (10)–(16) subject to the boundary conditions given in Eq. (17). Parametric continuation method is used to determine the solution of velocity components $f(\eta), f'(\eta)$, magnetic field components $M(\eta)$, $N(\eta)$, electric field components $H(\eta)$, $K(\eta)$, electric potential $m(\eta)$, and temperature distribution $\theta(\eta)$. Parametric analysis is carried out for the involved dimensionless parameters.

Main upshots of this paper are presented below:

- It is concluded that an increase in the magnitude of squeeze Reynolds number S leads to increase in fluid's density, which gives strength to the magnetic field from the lower plate to the upper plate.
- The Batchelor number decreases the strength of the horizontal component of magnetic field; this is due to the fact that magnetic field effect is weaker near the lower plate which is getting stronger as fluid moves towards the upper plate.
- Decreasing the mass diffusion decreases the anion distribution from the lower to the upper plate.
- Entropy generation and the Bejan number are maximum near the two plates because of the maximum disorderness due to plate movements and have minimum value in the fluid's center.
- Furthermore, the variations of entropy generation with an increasing value of the Prandtl number. It is analyzed that for a fixed value of domain, entropy generation amplifies with increase in P_r. Heat is a disorganized form of energy, and increasing the Eckert number increases viscous heating, therefore entropy production increases near the plates.

Acknowledgements
We thank the referees for pointing out some misprints and for helpful suggestions.

Funding
No funding has been received for this research work.

Abbreviations
p, pressure (N.m^{-2}); r, θ, z, cylindrical polar coordinates; u_r, radial velocity (m.s^{-1}); u_θ, azimuthal velocity (m.s^{-1}); u_z, axial velocity (m.s^{-1}); t, time (s); T_u, temperature at upper disc (K); T_l, temperature at lower disc (K); C_u, concentration at upper disc; C_l, concentration at lower disc; Pr, Prandtl number (ν/k); $\aleph_c$, strength of magnetic field; $\aleph_b$, squeezing parameter; $\aleph_d$, strength of magnetic field; $D(t)$, distance between two discs (m); B, induced magnetic field; δ_o, Soret number; λ, Dufour number; c_p, specific heat of fluid (J/kg K); D, molecular diffusion coefficient; k_T, thermal diffusion ratio; T_m, mean fluid

temperature (K); q_r, radiative heat flux (W/m^2); $\Re_d$, Radiative parameter; δ_c, Schmidt number; C, dimensional concentration; $\vec{r}$, radius vector of the disc; $\vec{V}$, velocity vector; ω, rotation vector; Ω_l, lower disc angular velocity; κ, thermal conductivity (W/m K); μ, dynamic viscosity (Pa S); ν, kinematic viscosity (kg/m S); σ, relative angular velocity; ρ, fluid density (kg/m^3); α, positive constant; η, similarity variable; Γ, transformed fluid temperature; σ^s, Stefan–Boltzmann constant; N_o, constant number; Ψ, transformed fluid concentration; κ^a, mean absorption co-efficient; u, fluid condition on upper disc; l, fluid condition on lower disc; $*$, dimensionless variable; $\prime$, derivative w.r.t. η.

Availability of data and materials
Data sharing not applicable to this article as no data sets were generated or analyzed during the current study.

Competing interests
The authors declare that they have no competing interests.

Authors' contributions
All authors have contributed equally in this paper. All authors read and approved the final manuscript.

Publisher's Note
Springer Nature remains neutral with regard to jurisdictional claims in published maps and institutional affiliations.

Received: 16 January 2019 Accepted: 4 June 2019 Published online: 20 June 2019

References

1. Hu, L., Harrison, J.D., Masliyah, J.H.: Numerical model of electrokinetic flow for capillary electrophoresis. J. Colloid Interface Sci. **215**, 300–312 (1999)
2. Mala, G.M., Li, D., Werner, C., Jacobasch, H.: Flow characteristics of water through a microchannel between two parallel plates with electrokinetic effects. Int. J. Heat Fluid Flow **18**, 489–496 (1997)
3. Arulanandam, S., Li, D.: Liquid transport in rectangular microchannels by electroosmotic pumping. Colloids Surf. A, Physicochem. Eng. Asp. **161**, 89–102 (2000)
4. Yang, R.J., Fu, L.M., Hwang, C.C.: Electroosmotic entry flow in a microchannel. J. Colloid Interface Sci. **244**, 173–179 (2001)
5. Hayes, M.A., Ewing, A.G.: Electroosmotic flow control and monitoring with an applied radial voltage for capillary zone electrophoresis. Anal. Chem. **64**, 512–516 (1992)
6. Ren, L., Li, D., Qu, W.: Electrokinetic flow through an elliptical microchannel: effects of aspect ratio and electrical boundary conditions. J. Colloid Interface Sci. **248**, 176–184 (2002)
7. Shah, R.A., Khan, A., Shuaib, M.: On the study of flow between unsteady squeezing rotating discs with cross diffusion effects under the influence of variable magnetic field. Heliyon **4**, e00925 (2018). https://doi.org/10.1016/j.heliyon.2018.e00925
8. Shah, R., Khan, A., Shuaib, M.: Analysis of squeezing flow of a viscous fluid between corotating discs with Soret and Dufour effects. Heat Transf. Res. **49**(11), 1103–1118 (2018)
9. Shah, R., Khan, A., Shuaib, M.: Dufour and Soret effect on heat and mass transfer with radiative heat flux in a viscous liquid over a rotating disk. Eur. Phys. J. Plus (2017). https://doi.org/10.1140/epjp/i2017-11632-4
10. Shah, R., Khan, A., Shuaib, F.: Convection from an infinite disk rotating in a vertical plane with variable magnetic force. J. Comput. Theor. Nanosci. **14**, 1–12 (2017)
11. Shah, R., Khan, A., Shuaib, M.: Study of second grade fluid over a rotating disk with Coriolis and centrifugal forces. J. Phys. Math. (2017). https://doi.org/10.4172/2090-0902.1000242
12. Shah, Z., Islam, S., Ayaz, H., Khan, S.: Radiative heat and mass transfer analysis of micropolar nanofluid flow of Casson fluid between two rotating parallel plates with effects of hall current. J. Heat Transf. **141**(2), 022401 (2018)
13. Shah, Z., Islama, S., Gul, T.: The electrical MHD and hall current impact on micropolar nanofluid flow between rotating parallel plates. Results Phys. **9**, 1201–1214 (2018)
14. Shah, Z., Islama, S., Gul, T.: Three dimensional third grade nanofluid flow in a rotating system between parallel plates with Brownian motion and thermophoresis effects. Results Phys. **10**, 36–45 (2018)
15. Shah, Z., Islama, S., Gul, T.: Darcy–Forchheimer flow of radiative carbon nanotubes with microstructure and inertial characteristics in the rotating frame. Case Stud. Therm. Eng. **12**, 823–832 (2018)
16. Khan, A., Shah, R.: Influence of cross-diffusion and radiation on mixed convection between rotating discs in the presence of a variable magnetic field. Eur. Phys. J. Plus **134**, 52 (2019). https://doi.org/10.1140/epjp/i2019-12396-5
17. Khan, A., Shah, R., Shuaib, M.: Fluid dynamics of the magnetic field dependent thermosolutal convection and viscosity between coaxial contracting discs. Results Phys. **9**, 923–938 (2018)
18. Lee, C.S., Blanchard, W.C., Wu, C.T.: Direct control of the electroosmosis in capillary zone electrophoresis by using an external electric field. Anal. Chem. **62**, 1550–1552 (1990)
19. Buch, J.S., Wang, P.C., DeVoe, D.L., Lee, C.S.: Field-effect flow control in a polydimethylsiloxane-based microfluidic system. Electrophoresis **22**, 3902–3907 (2001)
20. Mortensen, N.A., Olesen, L.H., Belmon, L., Bruus, H.: Electrohydrodynamics of binary electrolytes driven by modulated surface potentials. Phys. Rev. E **71**, 056306 (2005)
21. Gonzalez, A., Green, N.G., Ramos, A., Morgan, H., Castellanos, A.: Fluid flow induced by nonuniform ac electric fields in electrolytes on microelectrodes. II. A linear double layer theory. Phys. Rev. E **61**, 4019–4028 (2000)
22. Davidson, M.R., Harvie, D.J.E.: Electroviscous effects in low Reynolds number liquid flow through a slit-like microfluidic contraction. Chem. Eng. Sci. **62**, 4229–4240 (2007)
23. Liovic, P., Lakehal, D.: Multi-physics treatment in the vicinity of arbitrarily deformable gas–liquid interfaces. J. Comput. Phys. **222**, 504–535 (2007)
24. Park, H.M., Lee, J.S., Kim, T.W.: Comparison of the Nernst–Planck model and the Poisson–Boltzmann model for electroosmotic flows in microchannels. J. Colloid Interface Sci. **315**, 731–739 (2007)

25. Bharti, R.P., Harvie, D.J.E., Davidson, M.R.: Steady flow of ionic liquid through a cylindrical microfluidic contraction–expansion pipe: electroviscous effects and pressure drop. Chem. Eng. Sci. **63**, 3593–3604 (2008)
26. Rojas, G., Arcos, J., Peralta, M., Méndez, F., Bautista, O.: Pulsatile electroosmotic flow in a microcapillary with the slip boundary condition. Colloids Surf. A, Physicochem. Eng. Asp. **513**, 57–65 (2017)
27. Al-Odat, M., Damseh, R.A., Al-Nimr, M.A.: Effect of magnetic field on entropy generation due to laminar forced convection past a horizontal flat plate. Entropy **6**, 293–303 (2004)
28. Eegunjobi, A.S., Makinde, O.D.: Combined effect of buoyancy force and Navier slip on entropy generation in a vertical porous channel. Entropy **14**, 1028–1044 (2012)